



# Investigation of mechanical properties and stored elastic energy-fragmentation of $\text{Al}_2\text{O}_3$ - $\text{Cr}_2\text{O}_3$ ceramic system with increasing $\text{Cr}_2\text{O}_3$ content

Betül Kafkaslıoğlu Yıldız<sup>1,\*</sup>, Yahya Kemal Tür<sup>2</sup>

<sup>1</sup>Department of Metallurgical and Materials Engineering, Sivas University of Science and Technology, Sivas, 58000, Turkey

<sup>2</sup>Department of Materials Science and Engineering, Gebze Technical University, Gebze, 41420, Turkey

Received 28 February 2022; Received in revised form 7 July 2022; Accepted 14 October 2022

## Abstract

*In the present study, densification, mechanical properties (elastic modulus, hardness, flexural strength) and stored elastic energy-fragmentation of the pure  $\text{Al}_2\text{O}_3$  and  $\text{Al}_2\text{O}_3$ - $\text{Cr}_2\text{O}_3$  ceramics with different  $\text{Cr}_2\text{O}_3$  volume content (0.5, 1, 3, 5, 10 and 20 vol.%) were investigated. The fragmentation behaviour was interpreted from the point of armour application as larger fragments are required for higher penetration resistance. The equibiaxial flexural strength test method was used to measure the fracture strength values. A similar densification behaviour was obtained for the pure  $\text{Al}_2\text{O}_3$  and the  $\text{Al}_2\text{O}_3$ - $\text{Cr}_2\text{O}_3$  ceramic specimens with 0.5, 10 and 20 vol.%  $\text{Cr}_2\text{O}_3$  with the obtained relative densities of around 97%TD. The elastic modulus of the pure  $\text{Al}_2\text{O}_3$  and  $\text{Al}_2\text{O}_3$ - $\text{Cr}_2\text{O}_3$  ceramic specimens showed consistent values with the densification except for the  $\text{Al}_2\text{O}_3$ - $\text{Cr}_2\text{O}_3$  ceramics containing 20 vol.%  $\text{Cr}_2\text{O}_3$ . All  $\text{Al}_2\text{O}_3$ - $\text{Cr}_2\text{O}_3$  ceramics have lower flexural strength values than the pure  $\text{Al}_2\text{O}_3$ . The pure  $\text{Al}_2\text{O}_3$  had the smallest crack surface area accompanying the largest fragment size for given fracture energy. This indicates that the pure  $\text{Al}_2\text{O}_3$  will break into larger pieces in case of a possible impact.*

**Keywords:** alumina, chromium oxide, fracture strength, fragmentation, elastic energy

## I. Introduction

Chromia ( $\text{Cr}_2\text{O}_3$ ) is one of the additives that have the potential to improve physical properties of alumina ( $\text{Al}_2\text{O}_3$ ) ceramics for a variety of applications including military and biomedical areas [1,2].  $\text{Al}_2\text{O}_3$  and  $\text{Cr}_2\text{O}_3$  form isovalent solid solutions over the full range of compositions at high temperatures ( $T > 1000^\circ\text{C}$ ) as  $\text{Al}_2\text{O}_3$  and  $\text{Cr}_2\text{O}_3$  are sesquioxides with the same corundum crystal structure [3–5]. The substitution solid solution of  $\text{Cr}^{3+}$  ions in the  $\text{Al}_2\text{O}_3$  lattice is formed during the sintering stage through diffusion processes. It is stated in various studies that localized compressive stresses could be generated around the substituted  $\text{Cr}^{3+}$  ion because the radius of  $\text{Cr}^{3+}$  (0.076 nm) ions is larger than the  $\text{Al}^{3+}$  ions (0.068 nm) [1,6,7]. A hardening effect is reported in several studies for appropriate  $\text{Cr}^{3+}$

ion concentrations as a result of the generated compressive stress field that hinders the dislocation motion [6,8]. Also, Riu *et al.* [7] confirmed that a small amount of  $\text{Cr}_2\text{O}_3$  addition (~2 mol%) changed the morphology of  $\text{Al}_2\text{O}_3$  grains into plate-like due to the high diffusion rate of Cr ions through the surface of  $\text{Al}_2\text{O}_3$ . The fracture toughness was increased by the plate-like grains that generated the crack bridging toughening effect [7].

$\text{Cr}_2\text{O}_3$  is not stable in high oxygen partial pressure atmosphere. The evaporation of the composed Cr-containing species ( $\text{CrO}_3$ ) prevents the densification of the ceramic body as a result of the vaporization-condensation mechanism during sintering [4,9]. Azhar *et al.* [2] showed that the addition of 0.2–1.0 wt.%  $\text{Cr}_2\text{O}_3$  into  $\text{Al}_2\text{O}_3$  inhibited the densification after pressureless sintering in air at  $1600^\circ\text{C}$  for 4 h. However, solid solution formation could help densification by enhancing mass transport if sufficient formed solutions occur without evaporation [10]. Consequently, the evapo-

\*Corresponding author: tel: +90 542 724 12 74  
e-mail: [bkyildiz@sivas.edu.tr](mailto:bkyildiz@sivas.edu.tr)

ration of Cr-containing species is suppressed, and the densification process can be promoted.

Producing new composite systems and ceramics with low-cost equipment and processing techniques is a requirement to come through the insufficiency of monolithic ceramics used in armour technology [11]. There are some studies about the physical properties of the  $\text{Al}_2\text{O}_3$ - $\text{Cr}_2\text{O}_3$  ceramic system in the literature [2,4,5,12]. However, investigation of the crack length-stored energy relations by using elastic solutions to estimate deflection for  $\text{Al}_2\text{O}_3$ - $\text{Cr}_2\text{O}_3$  ceramic system comprising a wide volume range of  $\text{Cr}_2\text{O}_3$  additive was the motivation for this study. In their previous work, Kafkaslıoğlu Yıldız *et al.* [8] studied the effect of  $\text{Cr}_2\text{O}_3$  addition on the mechanical properties of the pure  $\text{Al}_2\text{O}_3$ , but they reported results for only three different volume ratios of  $\text{Cr}_2\text{O}_3$  (0.5, 1, 5 vol.%) and sub-micron sized (~200 nm)  $\text{Cr}_2\text{O}_3$  powder was used in the process.

In the present paper, the effects of six different  $\text{Cr}_2\text{O}_3$  volume contents (0.5, 1, 3, 5, 10 and 20 vol.%) on the microstructure, elastic modulus, hardness, flexural strength and fragmentation behaviour after equibiaxial bending loading of the pure  $\text{Al}_2\text{O}_3$  were investigated. The results obtained were interpreted for the use of the produced samples as a ceramic armour component especially in terms of fragmentation-elastic stored energy under equibiaxial bending loading. The equibiaxial flexural strength test could be utilized to analyse the fracture behaviour of a ceramic armour material owing to the similarity of fracture deformation after the ballistic impact [13]. The equibiaxial flexure strength test was used to investigate the stored elastic energy-fragmentation correlation of the  $\text{Al}_2\text{O}_3$ - $\text{Cr}_2\text{O}_3$  ceramic system with increasing  $\text{Cr}_2\text{O}_3$  content by considering the similar fracture deformation behaviour. As the high flexural strength is important for the structural integrity of a ceramic material, the study route was built on this mechanical property.

## II. Experimental

The precursors used in processing of the  $\text{Al}_2\text{O}_3$ - $\text{Cr}_2\text{O}_3$  samples included  $\alpha$ - $\text{Al}_2\text{O}_3$  ( $d_{50} = 0.5 \mu\text{m}$ ,  $d_{90} = 2.0 \mu\text{m}$ , 99.8% purity, Almatix Alumina CT3000 LS SG, Germany) and  $\text{Cr}_2\text{O}_3$  powder ( $D_{v,0.1} = 0.75 \mu\text{m}$ ,  $D_{v,0.5} = 1.46 \mu\text{m}$ ,  $D_{v,0.9} = 5.0 \mu\text{m}$  99% purity, Nanografi, Turkey). In addition, PVA, poly(vinyl alcohol) as the binder (Sigma Aldrich), glycerol as the plasticizer (Sigma Aldrich) and polyacrylic acid as the dispersant (Darvan 821A, MSE Tech Co. Ltd, Turkey) were used. Content of  $\text{Cr}_2\text{O}_3$  powder corresponding to 0.5, 1, 3, 5, 10 and 20 vol.% and polyacrylic acid were mixed for each ratio with the pure  $\text{Al}_2\text{O}_3$  in distilled water by ball milling for 24 h using  $\text{Al}_2\text{O}_3$  balls. Following the ball milling process, 2 wt.% binder solution (PVA + glycerol) was mixed with the prepared slurry and then dried on a hot plate below 90 °C. The powder was crushed in an agate mortar and sieved to 90  $\mu\text{m}$  before pressing.

Disc form specimens were prepared in a 35 mm diameter steel mould by uniaxial pressing at 40 MPa following 200 MPa cold isostatic pressing. The green  $\text{Al}_2\text{O}_3$ - $\text{Cr}_2\text{O}_3$  compacts were sintered at 1575 °C/2 h in 90% Ar + 10%  $\text{H}_2$  atmosphere in a tube furnace. Also, the pure  $\text{Al}_2\text{O}_3$  specimens were produced under the same conditions and sintered in air at 1550 °C/2 h with the same heating regime. The sintering temperatures of the pure  $\text{Al}_2\text{O}_3$  and  $\text{Al}_2\text{O}_3$ - $\text{Cr}_2\text{O}_3$  ceramics were tried to adjust for obtaining similar densification ratios. The production parameters (CIP pressure, sintering atmosphere etc.) were determined according to previous studies and the sintering temperature for the  $\text{Al}_2\text{O}_3$ - $\text{Cr}_2\text{O}_3$  ceramic samples was increased by 25 °C since high densities could not be obtained although finer  $\text{Cr}_2\text{O}_3$  powder size was used in the previous study [4,8].

In their previous work, Kafkaslıoğlu Yıldız *et al.* [8] studied the  $\text{Al}_2\text{O}_3$ - $\text{Cr}_2\text{O}_3$  ceramic samples with 0.5, 1 and 5 vol.%  $\text{Cr}_2\text{O}_3$  produced by using finer  $\alpha$ - $\text{Al}_2\text{O}_3$  powder ( $D = 0.25 \mu\text{m}$ ) and  $\text{Cr}_2\text{O}_3$  powders ( $D = 200 \text{nm}$ ), and polypropylene carbonate binder. Those specimens were sintered at 1550 °C/2 h in 90% Ar + 10%  $\text{H}_2$ . In the present study, starting powders particle sizes, binder system and sintering temperature were changed in addition to high  $\text{Cr}_2\text{O}_3$  content investigations. After sintering, all the specimens were ground by using a lapping machine with SiC abrasive powders (17  $\mu\text{m}$  and 9  $\mu\text{m}$  average particle size) to equalize the thickness of the disc formed specimens with nearly  $\pm 0.05 \text{mm}$  tolerance for more accurate elastic modulus and strength measurements. The final dimensions of the specimens were 28.3 mm in diameter and 2.30 mm in thickness with slight differences up to the composition. Following the lapping, the specimen surfaces were polished finally with a diamond solution for the hardness tests.

The bulk densities of the specimens were calculated through the measurement of macroscopic dimensions and weight. To compare the densification behaviour of the  $\text{Al}_2\text{O}_3$ - $\text{Cr}_2\text{O}_3$  ceramic specimens with the pure  $\text{Al}_2\text{O}_3$  and estimate the relative densities, theoretical densities of the compositions were determined according to the rule of mixtures even though it was not identified how much solid solution and evaporation occurred. The phase composition and crystalline structure of the specimens were analysed by X-ray diffraction method (Bruker® D8 Advance diffractometer) at a scanning rate of 4 °/min from 10° to 80°. Also, the highest intensity diffraction peak of the (104) crystal plane was examined at a scanning rate of 0.1 °/min from 34° to 36° to interpret the solid solution formation. The microstructure of thermally etched (for the pure  $\text{Al}_2\text{O}_3$  at 1450 °C/2 h in air, for the  $\text{Al}_2\text{O}_3$ - $\text{Cr}_2\text{O}_3$  ceramics at 1475 °C/2 h in 90% Ar + 10%  $\text{H}_2$ ) specimens and fracture surfaces were examined by scanning electron microscopy SEM (Philips XL 30 SFEG and TESCAN Mira3 XMU, Brno, Czech Republic). The linear intercept method was used to measure the grain size of the pure  $\text{Al}_2\text{O}_3$  and  $\text{Al}_2\text{O}_3$ - $\text{Cr}_2\text{O}_3$  ceramic specimens for all  $\text{Cr}_2\text{O}_3$  volume ratios.

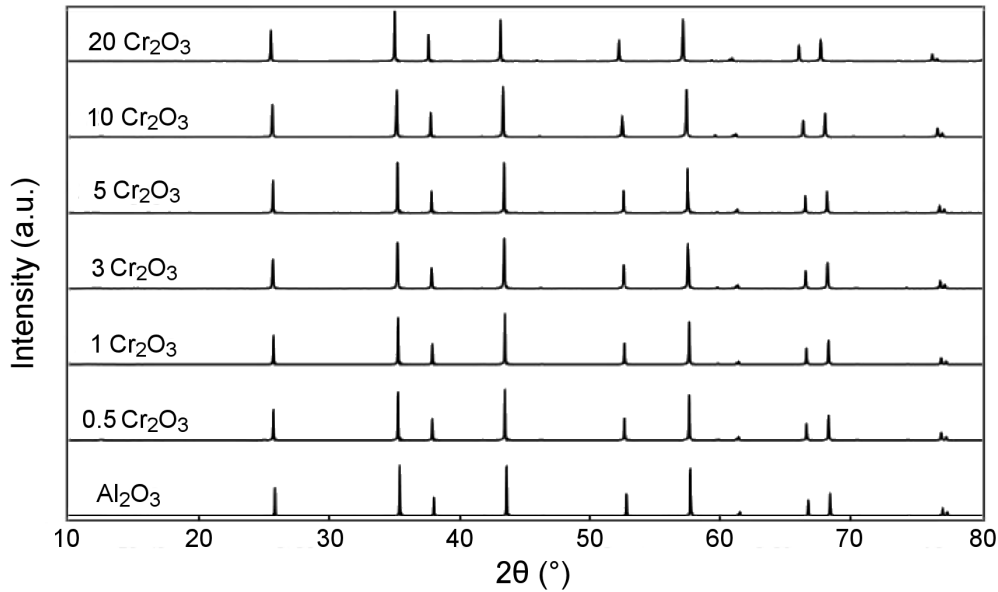


Figure 1. XRD patterns of the pure  $\text{Al}_2\text{O}_3$  and  $\text{Al}_2\text{O}_3\text{-Cr}_2\text{O}_3$  ceramics after sintering with different  $\text{Cr}_2\text{O}_3$  volume ratios

The elastic modulus measurements were performed consistent with an impulse excitation technique and ASTM E 1876 standard for disc-formed specimens in the GrindoSonic<sup>®</sup> Mk5 device. After the elastic modulus tests, the same ground and polished specimens were tested by using a monotonic equibiaxial flexural strength test (ring on ring) configuration with an Instron<sup>®</sup> 5569 tension/compression testing machine according to ASTM C 1499 standard to measure the fracture strength values and ten specimens were tested for each composition. The displacement rate was set as 0.3 mm/min and the diameters of the support ring and load ring were 23.9 mm and 9.8 mm, respectively. The specimens were photographed after the fracture strength tests to calculate the total crack lengths with ImageJ, image analysis software. For each specimen, the total measured crack length and specimen thickness were multiplied to find the total crack surface area values. Finally, hardness measurements were carried out on the broken pieces of the specimens by the Vickers indentation technique with an Instron<sup>®</sup> Wolpert Testor 2100 device under a 5 kg load.

### III. Results and discussion

X-ray diffraction patterns of the pure  $\text{Al}_2\text{O}_3$  and  $\text{Al}_2\text{O}_3\text{-Cr}_2\text{O}_3$  ceramic samples are given in Fig. 1. No new compound was identified after  $\text{Cr}_2\text{O}_3$  addition and solid solution formed due to the same corundum crystal structure of  $\text{Al}_2\text{O}_3$  and  $\text{Cr}_2\text{O}_3$  ceramics. All XRD peaks belong only to the corundum structure as expected. Since the radius of the chromium ion (0.076 nm) is larger than the radius of aluminium ion (0.068 nm), the incorporation of  $\text{Cr}^{3+}$  ions in  $\text{Al}_2\text{O}_3$  will increase the lattice dimensions. Consequently, the angle of X-ray diffraction peaks decreases consistently with Bragg's law [14,15]. The magnified XRD peak (corresponding

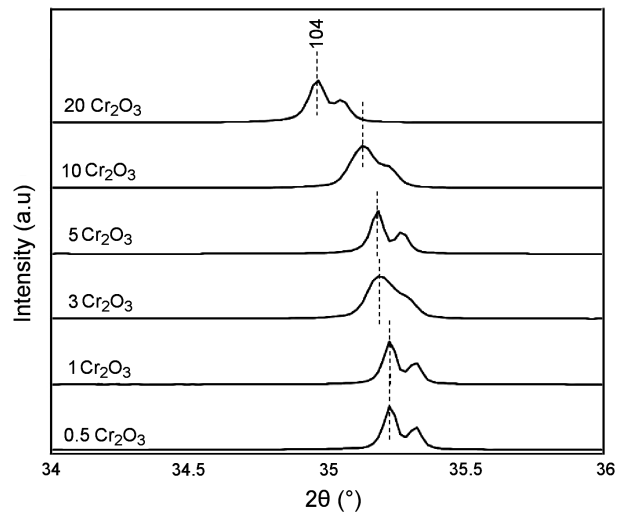


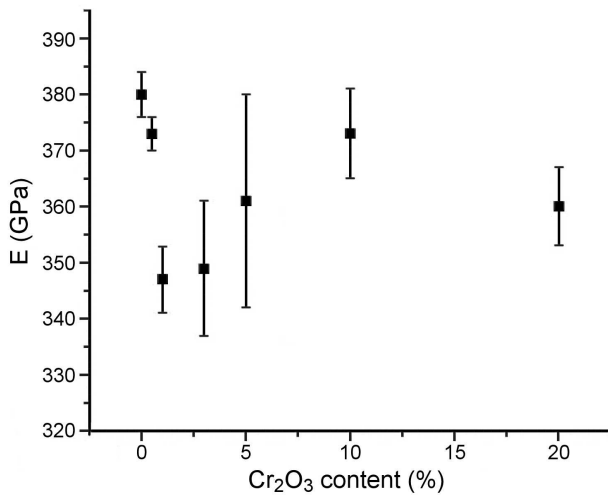
Figure 2. Change of XRD peaks between  $34^\circ\text{-}36^\circ$  with increasing  $\text{Cr}_2\text{O}_3$  volume ratio

to the (104) plane) in the range from  $34^\circ$  to  $36^\circ$  (Fig. 2) confirms the shift to the lower angles with an increasing  $\text{Cr}_2\text{O}_3$  volume ratio that is more prominent for the sample with 20 vol.%  $\text{Cr}_2\text{O}_3$ . This confirms the incorporation of  $\text{Cr}^{3+}$  in the structure and formation of  $\text{Al}_2\text{O}_3\text{-Cr}_2\text{O}_3$  solid solution [14].

All the measured physical and mechanical properties of the pure  $\text{Al}_2\text{O}_3$  and  $\text{Al}_2\text{O}_3\text{-Cr}_2\text{O}_3$  ceramic specimens are given in Table 1 (notation of the  $\text{Al}_2\text{O}_3\text{-Cr}_2\text{O}_3$  samples was abbreviated according to their  $\text{Cr}_2\text{O}_3$  content). High density (around 97 %TD) was obtained for the pure  $\text{Al}_2\text{O}_3$  and the  $\text{Al}_2\text{O}_3\text{-Cr}_2\text{O}_3$  ceramic specimens with 0.5, 10 and 20 vol.%  $\text{Cr}_2\text{O}_3$ . Even though the  $\text{Al}_2\text{O}_3\text{-Cr}_2\text{O}_3$  ceramic specimens were sintered at a higher temperature than the pure  $\text{Al}_2\text{O}_3$ , the densification was insufficient.  $\text{Cr}_2\text{O}_3$  is susceptible to evaporation at very low oxygen partial pressures and

**Table 1.** The measured physical and mechanical properties of the pure Al<sub>2</sub>O<sub>3</sub> and Al<sub>2</sub>O<sub>3</sub>-Cr<sub>2</sub>O<sub>3</sub> ceramics

Material	Relative density [%]	Elastic modulus [GPa]	Grain size [μm]	Hardness [GPa]	Flexural strength [MPa]	Weibull modulus	Weibull strength [MPa]
Al <sub>2</sub> O <sub>3</sub>	97.3 ± 0.8	380 ± 4	1.04	19.50 ± 1.0	350 ± 30	15	362
0.5 Cr <sub>2</sub> O <sub>3</sub>	97.0 ± 0.4	373 ± 3	2.66	17.53 ± 1.1	322 ± 28	14	334
1 Cr <sub>2</sub> O <sub>3</sub>	94.8 ± 1.0	347 ± 6	3.08	17.52 ± 0.9	296 ± 30	15	308
3 Cr <sub>2</sub> O <sub>3</sub>	94.4 ± 2.0	349 ± 12	4.38	17.36 ± 0.2	298 ± 31	13	310
5 Cr <sub>2</sub> O <sub>3</sub>	95.4 ± 2.0	361 ± 19	3.60	16.91 ± 0.9	278 ± 63	7	300
10 Cr <sub>2</sub> O <sub>3</sub>	97.6 ± 0.9	373 ± 8	4.43	16.65 ± 0.6	269 ± 77	4	296
20 Cr <sub>2</sub> O <sub>3</sub>	97.0 ± 0.6	359 ± 7	5.00	16.41 ± 1.0	288 ± 50	8	307

**Figure 3.** Elastic modulus values of the pure Al<sub>2</sub>O<sub>3</sub> and the Al<sub>2</sub>O<sub>3</sub>-Cr<sub>2</sub>O<sub>3</sub> ceramics with different Cr<sub>2</sub>O<sub>3</sub> content

the evaporation-condensation sintering mechanism of Cr<sub>2</sub>O<sub>3</sub> hinders obtaining of dense bodies. In addition, solid solution formation could consume extra heat energy that leads to ceramics with low densification after sintering [3]. These conditions were valid, especially with moderate (1, 3 and 5%) Cr<sub>2</sub>O<sub>3</sub> volume content. Conversely, solid solution formation could enhance mass transport, and this was valid for the Al<sub>2</sub>O<sub>3</sub>-Cr<sub>2</sub>O<sub>3</sub> ceramic system with high Cr<sub>2</sub>O<sub>3</sub> content to some extent. The correlation of elastic modulus with Cr<sub>2</sub>O<sub>3</sub> content is given in Fig. 3. The elastic modulus of the pure Al<sub>2</sub>O<sub>3</sub> and Al<sub>2</sub>O<sub>3</sub>-Cr<sub>2</sub>O<sub>3</sub> ceramic specimens showed consistent values with the densification (i.e. lower relative density results in lower elastic modulus) except for the Al<sub>2</sub>O<sub>3</sub>-Cr<sub>2</sub>O<sub>3</sub> ceramics containing 20 vol.% of Cr<sub>2</sub>O<sub>3</sub>. The elastic modulus of Cr<sub>2</sub>O<sub>3</sub> is about 280 GPa, so higher Cr<sub>2</sub>O<sub>3</sub> content also affected the modulus value negatively.

Figure 4 shows the SEM micrographs of the thermally etched pure Al<sub>2</sub>O<sub>3</sub> and the Al<sub>2</sub>O<sub>3</sub>-Cr<sub>2</sub>O<sub>3</sub> ceramic samples. There is no evidence of impurity phase and the solvated Cr<sub>2</sub>O<sub>3</sub> additive could not be distinguished separately as all dark grains belong to the corundum phase. The average grain sizes of the compositions, measured by the linear intercept method, are given in Table 1. The growth of Al<sub>2</sub>O<sub>3</sub> grains was apparent for all compositions containing Cr<sub>2</sub>O<sub>3</sub> additive, especially for the sample containing 20 vol.% Cr<sub>2</sub>O<sub>3</sub> having the average grain size of ~5 μm. Since the sintering temperature of

the pure Al<sub>2</sub>O<sub>3</sub> was 25 °C lower than the Al<sub>2</sub>O<sub>3</sub>-Cr<sub>2</sub>O<sub>3</sub> ceramics, the smaller size of the Al<sub>2</sub>O<sub>3</sub> grain could be expected. However, similar and lower densification of the Al<sub>2</sub>O<sub>3</sub>-Cr<sub>2</sub>O<sub>3</sub> ceramic specimens do not affect the grain growth tendency. While a solid solution formed, the presence of Cr<sup>3+</sup> ions brought an increase in the growth rate of Al<sub>2</sub>O<sub>3</sub> grains due to the coherency strain energy at the grain boundary [7]. It is stated that a chemically induced grain boundary migration can happen in solid solutions if there is grain boundary mobility at a high enough temperature [16]. Rapid migration of grain boundaries through coherency strain energy results in changes in the microstructure such as the formation of plate-like grains [7].

Figure 5 shows the flexural strength of the pure Al<sub>2</sub>O<sub>3</sub> and Al<sub>2</sub>O<sub>3</sub>-Cr<sub>2</sub>O<sub>3</sub> ceramics. In addition, Weibull plots of the obtained samples are shown in Fig. 6 and Weibull modulus and Weibull strength data are presented in Table 1. All Al<sub>2</sub>O<sub>3</sub>-Cr<sub>2</sub>O<sub>3</sub> ceramics have lower flexural strength values than the pure Al<sub>2</sub>O<sub>3</sub> even for the samples with density similar to that of the pure Al<sub>2</sub>O<sub>3</sub>. The decrease in strength can be attributed to the increase in grain size for the Cr<sub>2</sub>O<sub>3</sub> containing ceramics. According to Tuan *et al.* [17], the strength of ceramic material is inversely proportional to the flaw size. The lower strength values for the Al<sub>2</sub>O<sub>3</sub>-Cr<sub>2</sub>O<sub>3</sub> ceramics are related to the larger flaw size due to lower densification. Weibull modulus, *m*, is a measure of the scatter in strength values and higher *m* values point to more homogeneous specimens [18]. Higher amount of Cr<sub>2</sub>O<sub>3</sub> (i.e. 5, 10 and 20 vol.%) adversely affected the homogeneity of materials independent of densification. The highest characteristic strength and the most consistent strength values were obtained for the pure Al<sub>2</sub>O<sub>3</sub>.

Figure 7 illustrates the fracture surfaces' SEM micrographs of the pure Al<sub>2</sub>O<sub>3</sub> and Al<sub>2</sub>O<sub>3</sub>-Cr<sub>2</sub>O<sub>3</sub> ceramic samples after the equibiaxial flexural strength test (the transgranular regions are circled and the intergranular regions are indicated by arrows). The pure Al<sub>2</sub>O<sub>3</sub> has mainly intergranular fracture mode with some areas that have cleavage fracture behaviour. Although there are slight differences depending on where the image was taken, the fracture mode changed from intergranular to mostly transgranular with some intergranular areas after the Cr<sub>2</sub>O<sub>3</sub> addition. The energy required for transgranular fracture is higher than the energy needed for intergranular [19]. Thus, the fracture mode change points

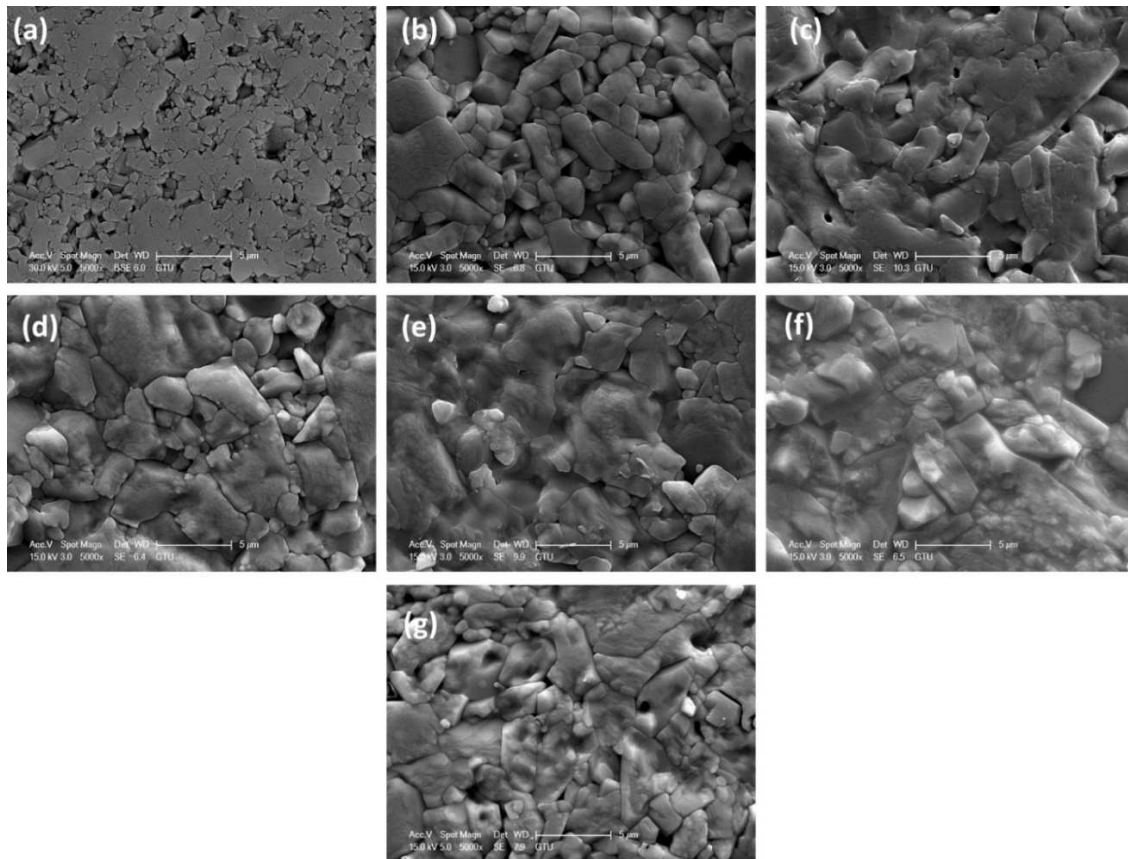


Figure 4. Thermally etched SEM micrographs of pure  $\text{Al}_2\text{O}_3$  (a) and samples with: b) 0.5, c) 1, d) 3, e) 5, f) 10 and g) 20 vol.%  $\text{Cr}_2\text{O}_3$

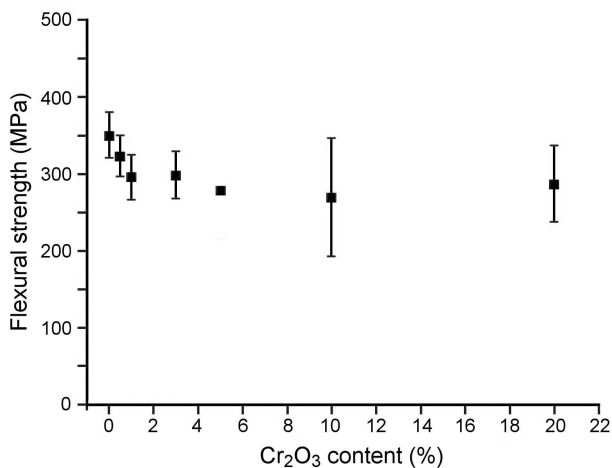


Figure 5. Flexural strength as a function of  $\text{Cr}_2\text{O}_3$  content

to the increase in the strength of the ceramic material in general. However, low densification rates and large porosities caused low flexural strength values for the  $\text{Al}_2\text{O}_3$ - $\text{Cr}_2\text{O}_3$  ceramics through fracture mode change.

Besides the elastic modulus and flexural strength, hardness is also adversely affected by high porosity. Vickers hardness values of the pure  $\text{Al}_2\text{O}_3$  and  $\text{Al}_2\text{O}_3$ - $\text{Cr}_2\text{O}_3$  ceramics are shown in Table 1. Although, the 0.5, 10 and 20 vol.%  $\text{Cr}_2\text{O}_3$  containing  $\text{Al}_2\text{O}_3$ - $\text{Cr}_2\text{O}_3$  samples have similar densification with the pure  $\text{Al}_2\text{O}_3$ , their hardness values were lower than the pure  $\text{Al}_2\text{O}_3$

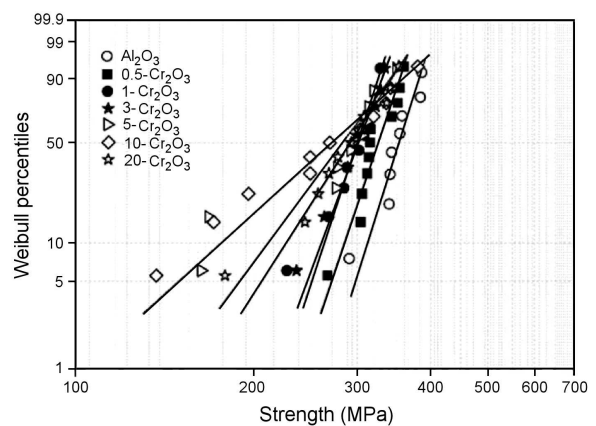


Figure 6. Weibull plots of the compositions with different  $\text{Cr}_2\text{O}_3$  content

indicating the existence of large porosities in the  $\text{Cr}_2\text{O}_3$  containing specimens.

In a ballistic impact occurrence on the front of a ceramic armour material, fracture into larger fragments is essential due to larger fractured pieces being a harder barrier on the way of the striking penetrator. This results in more abrasion and higher resistance for multi-hit capability [20]. Therefore, the size of broken pieces, i.e. the fragmentation mode has great importance for ceramic armour performance. Figure 8 shows the relationship between the stored elastic energy (J) and the total crack surface area ( $\text{mm}^2$ ) with the linear fit lines for

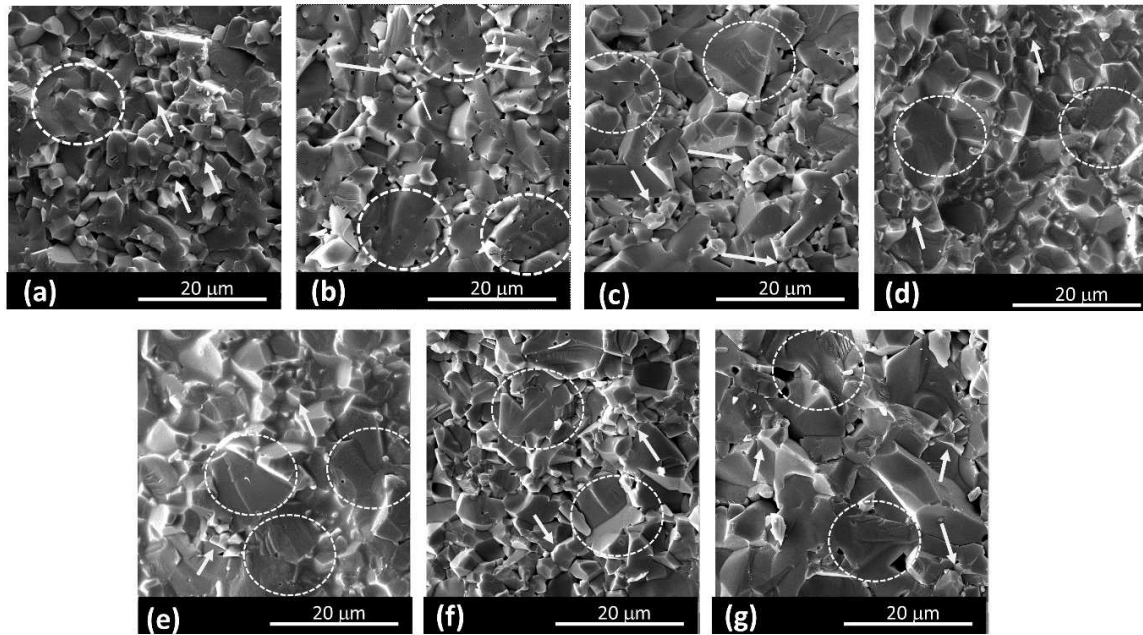


Figure 7. Fracture surfaces SEM micrograph of pure  $\text{Al}_2\text{O}_3$  (a) and samples with: b) 0.5, c) 1, d) 3, e) 5, f) 10 and g) 20 vol.%  $\text{Cr}_2\text{O}_3$

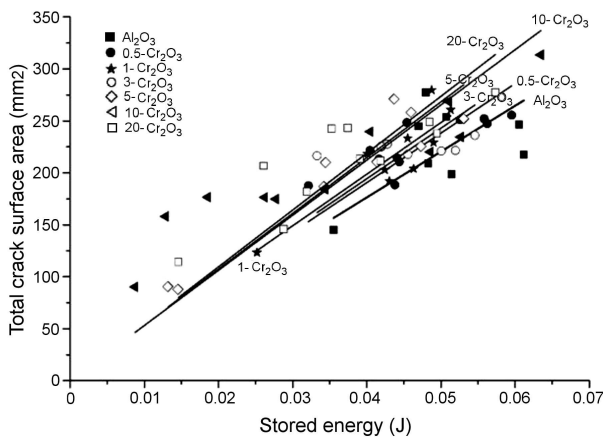


Figure 8. The total crack surface area dependence on the stored energy for the pure  $\text{Al}_2\text{O}_3$  and the  $\text{Al}_2\text{O}_3$ - $\text{Cr}_2\text{O}_3$  ceramics

the pure  $\text{Al}_2\text{O}_3$  and  $\text{Al}_2\text{O}_3$ - $\text{Cr}_2\text{O}_3$  ceramics. The linear fit lines were adjusted for passing through the origin, i.e. zero crack surface area at zero stored energy. It can be seen that the crack surface area is directly proportional to the stored energy even though there is an extensive scatter for both the stored energy and the total crack surface area in all the compositions. Deformation is elastic for a ceramic material in quasi-static bending conditions; so, the stored elastic energy is equivalent to the work done by the load. The work done by the load can be calculated from the area ( $W = 1/2F\Delta$ ) below the linear load-displacement ( $F$ - $\Delta$ ) curve [21]. The displacement of the disc formed specimen during an equibiaxial flexural strength test can be predicted by using the symmetric flexure of circular plates' solutions. At the radius equal to the loading ring, the displacement of the concentrically loaded simply supported plate can

be calculated with the equations given by Timoshenko [22]. As it can be seen in Fig. 8, the pure  $\text{Al}_2\text{O}_3$  has the lowest linear fit line slope. However, 5, 10 and 20 vol.%  $\text{Cr}_2\text{O}_3$  containing  $\text{Al}_2\text{O}_3$ - $\text{Cr}_2\text{O}_3$  ceramic specimens have nearly the same highest slope. The 0.5, 1 and 3 vol.%  $\text{Cr}_2\text{O}_3$  containing specimens' slope lay in between. The lowest slope means that the pure  $\text{Al}_2\text{O}_3$  would have the smallest total crack surface area accompanying the largest fragment size for given fracture energy between all the ceramics. High flexural strength values resulted in a large fragmentation size for the pure  $\text{Al}_2\text{O}_3$  specimens.

#### IV. Conclusions

The  $\text{Al}_2\text{O}_3$ - $\text{Cr}_2\text{O}_3$  ceramics with different  $\text{Cr}_2\text{O}_3$  content (0.5, 1, 3, 5, 10 and 20 vol.%) were produced by pressureless sintering in 10%  $\text{H}_2$ /90% Ar at 1575 °C/2 h to investigate the effects of  $\text{Cr}_2\text{O}_3$  on the microstructure, mechanical properties and especially fragmentation behaviour of the pure  $\text{Al}_2\text{O}_3$  that was sintered in air at 1550 °C/2 h. The stored elastic energy-total crack surface area relation was used to evaluate the possible fragmentation behaviour of the produced ceramics under impact. Relative density of around 97 %TD was obtained for the pure  $\text{Al}_2\text{O}_3$  and  $\text{Al}_2\text{O}_3$ - $\text{Cr}_2\text{O}_3$  ceramics with 0.5, 10 and 20 vol.%  $\text{Cr}_2\text{O}_3$  content. However, densities of the 1, 3 and 5 vol.%  $\text{Cr}_2\text{O}_3$  containing specimens were lower. The elastic modulus of the pure  $\text{Al}_2\text{O}_3$  and  $\text{Al}_2\text{O}_3$ - $\text{Cr}_2\text{O}_3$  specimens showed consistent values with the densification except for the  $\text{Al}_2\text{O}_3$ - $\text{Cr}_2\text{O}_3$  containing 20 vol.%  $\text{Cr}_2\text{O}_3$ . Although, the 0.5, 10, 20 vol.%  $\text{Cr}_2\text{O}_3$  containing  $\text{Al}_2\text{O}_3$ - $\text{Cr}_2\text{O}_3$  have similar densification to the pure  $\text{Al}_2\text{O}_3$ , their hardness values were lower than that of the pure  $\text{Al}_2\text{O}_3$ . In addition, all  $\text{Al}_2\text{O}_3$ -

Cr<sub>2</sub>O<sub>3</sub> ceramics have lower flexural strength values than the pure Al<sub>2</sub>O<sub>3</sub> and low densification rates with large porosities caused low flexural strength for the Al<sub>2</sub>O<sub>3</sub>-Cr<sub>2</sub>O<sub>3</sub> ceramics though fracture mode changed. For a given stored energy, the pure Al<sub>2</sub>O<sub>3</sub> would have the smallest total crack surface concomitant to the largest fragment size among all the compositions. The expected strength improvement and fracture behaviour could not be obtained from the Al<sub>2</sub>O<sub>3</sub>-Cr<sub>2</sub>O<sub>3</sub> ceramics sintered in H<sub>2</sub>/Ar atmosphere for 1575 °C/2h prepared with presently used Cr<sub>2</sub>O<sub>3</sub> powder size.

**Acknowledgments:** The support of Sivas University of Science and Technology Scientific Research Council to project with grant number 2020-GENL-Müh-0006 is greatly appreciated. The authors also thank Ahmet Nazım with Halil İbrahim Çetintaş and Adem Şen for their assistance in the SEM and XRD analysis of this research, respectively.

## References

1. M. Kuntz, R. Krüger, “The effect of microstructure and chromia content on the properties of zirconia toughened alumina”, *Ceram. Int.*, **44** (2018) 2011–2020.
2. A.Z.A. Azhar, L.C. Choong, H. Mohamed, M.M. Ratnam, Z.A. Ahmad, “Effects of Cr<sub>2</sub>O<sub>3</sub> addition on the mechanical properties, microstructure and wear performance of zirconia-toughened-alumina (ZTA) cutting inserts”, *J. Alloys Compd.*, **513** (2012) 91–96.
3. M. Nath, P. Kumar, A.V. Maldhure, S. Sinhamahapatra, K. Dana, A. Ghosh, H.S. Tripathi, “Anomalous densification behavior of Al<sub>2</sub>O<sub>3</sub>-Cr<sub>2</sub>O<sub>3</sub> system”, *Mater. Character.*, **111** (2016) 8–13.
4. M. Nath, S. Sen, K. Banerjee, A. Ghosh, H.S. Tripathi, “Densification behavior and properties of alumina-chrome ceramics: effect of TiO<sub>2</sub>”, *Ceram. Int.*, **39** (2013) 227–232.
5. K. Cui, T. Fu, Y. Zhang, J. Wang, H. Mao, T. Tan, “Microstructure and mechanical properties of CaAl<sub>12</sub>O<sub>19</sub> reinforced Al<sub>2</sub>O<sub>3</sub>-Cr<sub>2</sub>O<sub>3</sub> composites”, *J. Eur. Ceram. Soc.*, **41** (2021) 7935.
6. C.L. Li, D.H. Riu, T. Sekino, K. Niihara, “Fabrication and mechanical properties of Al<sub>2</sub>O<sub>3</sub> solid solution with low addition of Cr<sub>2</sub>O<sub>3</sub>”, *Key Eng. Mater.*, **161-163** (1999) 161–164.
7. D.H. Riu, Y.M. Kong, H.E. Kim, “Effect of Cr<sub>2</sub>O<sub>3</sub> addition on microstructural evolution and mechanical properties of Al<sub>2</sub>O<sub>3</sub>”, *J. Eur. Ceram. Soc.*, **20** (2000) 1475–1481.
8. B. Kafkaslıoğlu Yıldız, H. Yılmaz, Y.K. Tür, “Evaluation of mechanical properties of Al<sub>2</sub>O<sub>3</sub>-Cr<sub>2</sub>O<sub>3</sub> ceramic system prepared in different Cr<sub>2</sub>O<sub>3</sub> ratios for ceramic armour components”, *Ceram. Int.*, **45** (2019) 20575–20582.
9. T. Hirata, K. Akiyama, H. Yamamoto, “Sintering behavior of Cr<sub>2</sub>O<sub>3</sub>-Al<sub>2</sub>O<sub>3</sub> ceramics”, *J. Eur. Ceram. Soc.*, **20** (2000) 195–199.
10. X.G. Wang, J.X. Liu, Y.M. Kan, G.J. Zhang, “Effect of solid solution formation on densification of hot-pressed ZrC ceramics with MC (M = V, Nb, and Ta) additions”, *J. Eur. Ceram. Soc.*, **32** (2012) 1795–1802.
11. E. Medvedovski, “Ballistic performance of armour ceramics: influence of design and structure. Part 1”, *Ceram. Int.*, **36** (2010) 2103–2115.
12. K. Cui, Y. Zhang, T. Fu, S. Hussain, T. Saad Algarni, J. Wang, X. Zhang, S. Ali, “Effects of Cr<sub>2</sub>O<sub>3</sub> content on microstructure and mechanical properties of Al<sub>2</sub>O<sub>3</sub> matrix composites”, *Coatings*, **11** (2021) 234.
13. A. Healey, J. Cotton, S. Maclachlan, P. Smith, J. Yeomans, “Understanding the ballistic event: methodology and initial observations”, *J. Mater. Sci.*, **52** (2017) 3074–3085.
14. P. Zhao, H. Zhao, J. Yu, H. Zhang, H. Gao, Q. Chen, “Crystal structure and properties of Al<sub>2</sub>O<sub>3</sub>-Cr<sub>2</sub>O<sub>3</sub> solid solutions with different Cr<sub>2</sub>O<sub>3</sub> contents”, *Ceram. Int.*, **44** (2018) 1356–1361.
15. J.F. Xia, H.Q. Nian, W. Liu, X.G. Wang, D.Y. Jiang, “Effect of Cr<sub>2</sub>O<sub>3</sub> derived from Cr(NO<sub>3</sub>)<sub>3</sub>·9H<sub>2</sub>O precursor on the densification and mechanical properties of zirconia toughened alumina (ZTA) composites”, *Ceram. Int.*, **42** (2016) 9116–9124.
16. S.C. Han, D.K. Yoon, M.K. Brun, “Migration of grain boundaries in alumina induced by chromia addition”, *Acta Metall. Mater.*, **43** (1995) 977–984.
17. W.H. Tuan, J.R. Chen, C.J. Ho, “Critical zirconia amount to enhance the strength of alumina”, *Ceram. Int.*, **34** (2008) 2129–2135.
18. B. Kafkaslıoğlu Yıldız, H. Yılmaz, Y.K. Tür, “Processing and mechanical characterization of Al<sub>2</sub>O<sub>3</sub>/Ni and Al<sub>2</sub>O<sub>3</sub>/Co composites by pressureless sintering of nanocomposite powders”, *Process. Appl. Ceram.*, **12** [2] (2018) 123–128.
19. T. Rodriguez-Suarez, J.F. Bartolomé, A. Smirnov, S. Lopez-Esteban, R. Torrecillas, J.S. Moya, “Sliding wear behaviour of alumina/nickel nanocomposites processed by a conventional sintering route”, *J. Eur. Ceram. Soc.*, **31** (2011) 1389–1395.
20. D.B. Rahbek, B.B. Johnsen, *Dynamic Behaviour of Ceramic Armour Systems*, Norwegian Defence Research Establishment (FFI), 2015.
21. B. Kafkaslıoğlu Yıldız, Y.K. Tür, “An investigation of equibiaxial flexural strength and hardness properties of Al<sub>2</sub>O<sub>3</sub>-Ni nanocomposites based microstructures with ZrO<sub>2</sub> and Cr<sub>2</sub>O<sub>3</sub> additives”, *Mater. Sci. Eng. A*, **758** (2019) 103–111.
22. S. Timoshenko, S. Woinowsky-Krieger, *Theory of Plates and Shells*, 2<sup>nd</sup> Ed., McGraw-Hill Book Company, USA, 1959.